

Capillary rupture of suspended polymer concentric rings

Zheng Zhang and Ronggui Yang

Department of Mechanical Engineering,

University of Colorado at Boulder, Boulder, Colorado 80309, USA

G. C. Hilton

National Institute of Standards and Technology, Boulder, Colorado 80305, USA

Yifu Ding*

Department of Mechanical Engineering,

University of Colorado at Boulder, Boulder, Colorado 80309, USA and

Materials Science and Engineering Program,

University of Colorado at Boulder, Boulder, Colorado 80309, USA

(Dated: August 15, 2024)

Abstract

We present the first experimental study on the simultaneous capillary instability amongst viscous concentric rings suspended atop an immiscible medium. The rings ruptured upon annealing, with three types of phase correlation between neighboring rings. In the case of weak substrate confinement, the rings ruptured independently when they were sparsely distanced, but via an out-of-phase mode when packed closer. If the substrate confinement was strong, the rings would rupture via an in-phase mode, resulting in radially aligned droplets. The concentric ring geometry caused a competition between the phase correlation of neighboring rings and the kinetically favorable wavelength, yielding an intriguing, recursive surface pattern. This frustrated pattern formation behavior was accounted for by a scaling analysis.

Capillary instability is a commonly observed phenomenon: a slender liquid object ruptures into a series of droplets, driven by surface/interfacial tension (γ) [1]. The droplets are spaced at a characteristic distance, corresponding to the fastest growing wavelength (mode). From Tomotika’s linear stability analysis, this mode is a function of the interfacial tension and the cylinder-to-medium viscosity ratio [2]. When multiple cylinders are embedded in parallel within the same medium, the dominant mode for neighboring cylinders can become correlated [3]: the droplets positioned either in-phase or out-of-phase [4].

Instability of non-minimal shapes is fundamentally interesting. However, despite the rich literature on capillary instability of straight cylinders, studies on curved objects have been rather lacking until recent years. Pairam et al. [5] successfully created an unstable ring (toroid) by injecting liquid into a rotating bath of an immiscible liquid. They showed that the evolution of the as-formed ring was dictated by the competition between radial contraction and circumferential rupture [5]. Yao et al. analyzed the Stokes flow during the contraction [6]. Mehrabian et al. simulated both the contraction and the non-linear rupture of an embedded Newtonian ring [7]. The aforementioned literature suggests that the characteristic contraction time and rupture time predominantly scale with the medium viscosity and ring viscosity, respectively. Indeed, by replacing the medium with a highly viscoelastic material, the two timescales can be decoupled [8]. Furthermore, the stability of a substrate-supported liquid ring was studied both theoretically [9] and experimentally, via spin-coating [10], solvent evaporation [11] and pulse-laser [12, 13], as well as ion-beam [14].

Previous research has focused on a single ring; whether and how multiple closely arranged rings would rupture remained unclear. This could be because none of the literature methods were capable of creating multiple embedded rings, with well-defined dimensions and physical properties. In this Letter, we report the first experimental study on capillary instability amongst suspended concentric rings.

The concentric rings were created by a three-step fabrication process, which we developed previously [15]. Briefly, we first imprint a concentric ring pattern on a spin-coated poly(methyl methacrylate) (PMMA) film, via nanoimprint lithography. Next, a layer of polystyrene (PS) was spin-coated onto the PMMA pattern, using a selective solvent (1-chloropentane). The bilayer would form individual rings upon annealing. In this Letter, we show three representative samples (A, B and C), imprinted with different patterns.

The cross-sectional geometry of the as-cast patterns is illustrated in Fig. 1(a1), where PS

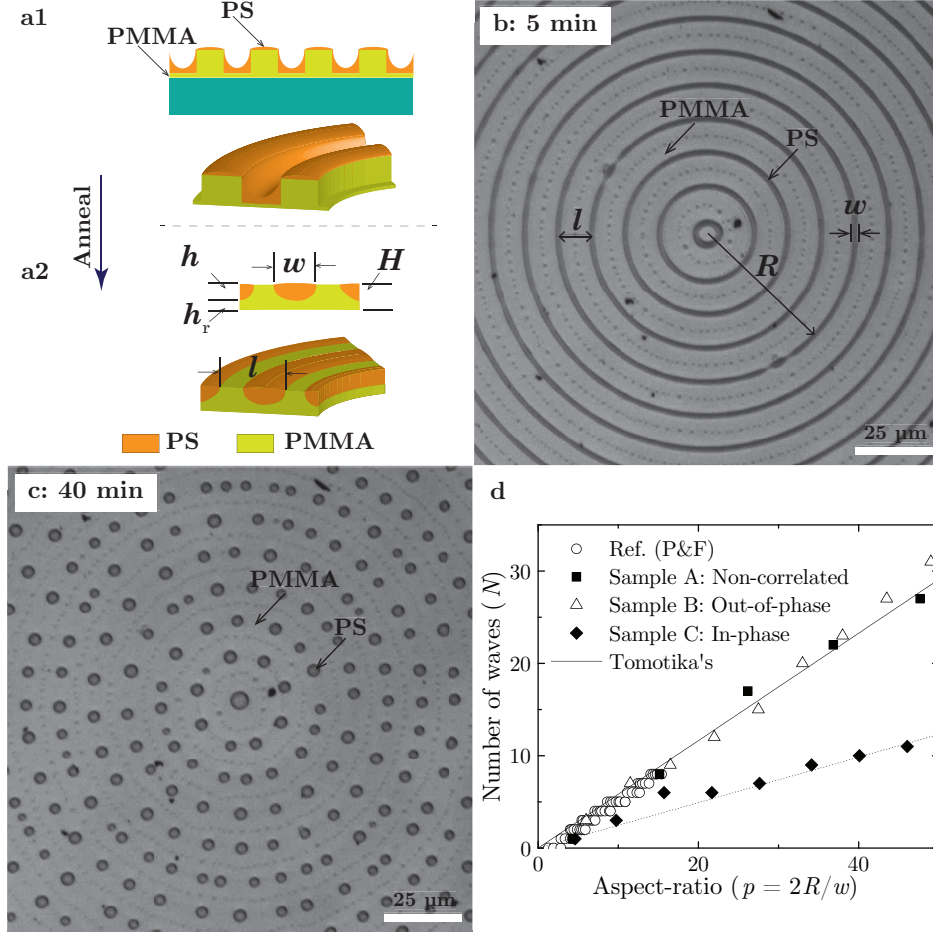


Figure 1. (a1-a2) Schematic of the formation of suspended PS rings upon annealing. Optical image of concentric PS rings ($w = 3.1 \mu\text{m}$, $l = 20.2 \mu\text{m}$, Sample A) (b) as formed and (c) after rupture, annealed at $160 \text{ }^\circ\text{C}$ for the labeled durations. (d) The number of capillary waves plotted as a function of aspect ratio. The solid line is based on Tomotika's theory. The dotted line is a linear fit to the ‘‘In-phase’’ data. The empty circles are adapted from reference [5].

mostly segregated in the PMMA trenches. Being a non-minimum shape, the pattern would spontaneously evolve at a temperature above the T_g s of PS and PMMA.

At first, the corrugation was leveled by the vertical Laplace pressure ($P \approx 2\pi^2\gamma d/l^2$, where d and l are the height and periodicity of the corrugation, respectively [16, 17]), forming PS rings atop PMMA. Hereafter we refer to the PS rings as the ‘‘rings’’. Fig. 1(a2) schematically shows the cross-section of the rings, with w , h , h_r denoting the width and thickness of the ring, and the residual layer thickness, respectively.

At $160 \text{ }^\circ\text{C}$, the entire leveling process completed within the first minute of annealing, as

the flow times of both polymers under P were very short: $\eta_{\text{PS}} = 802 \text{ Pa} \cdot \text{s}$, and $\eta_{\text{PMMA}} = 1450 \text{ Pa} \cdot \text{s}$, from our rheological measurements. During this process, w of the rings decreased, in order to balance the surface tension of PS and the interfacial tension of PS/PMMA ($\gamma_{\text{PS}}/\gamma_{\text{PS/PMMA}} \approx 24$) [15, 18]. The R of each ring and periodicity l remained nearly constant, indicating negligible contraction of the rings. The only exception was the innermost ring in Fig. 1b evolving into a single droplet in Fig. 1c. However, this was not due to radial contraction: the ring ruptured first and then rounded up (Fig. S2), which was also observed on fat rings by Pairam et al. [5]

By adopting Yao & Bowick’s solution [6], the contraction rate for the 2nd innermost ring was estimated to be on the order of $10^{-3} \mu\text{m/s}$. Before the capillary rupture time of $\sim 20 \text{ min}$ (Fig. S2c), R would only decrease $\sim 1 \mu\text{m}$, which was negligible in comparison with l . The rest of the rings had even larger aspect-ratio ($p = 2R/w$) and, therefore, even smaller contraction rate. Here $w/2$ is considered equivalent to the tube radius (a) of a toroid. In following discussions, we will only focus on the rupture behaviors of the rings, after the initial leveling process.

Fig. 1b shows Sample A at 5 min of annealing, forming concentric rings with $w \approx 3.1 \mu\text{m}$, $h \approx 1.0 \mu\text{m}$, $h_r \approx 1.1 \mu\text{m}$ and $l \approx 20.2 \mu\text{m}$. All the rings had identical w , which guaranteed $p \propto R$. The cross-section of each ring, represented by a ratio of $w/h \approx 3$, is consistent with that of straight filaments after the fast leveling process [15, 19, 20]. At this time, the rings in the PMMA trenches remained continuous, albeit periodic capillary fluctuations were already discernible (Fig. 1b). After 40 min, all rings had ruptured into discrete droplets (Fig. 1c). Note that the ruptured segments quickly equilibrated into droplets and were kinetically immobilized, because collision-based coalescence rate was extremely slow.

We plot the number of waves (N) from each ring as a function of p (solid squares in Fig. 1d). The relationship agrees well with Tomotika’s theory for a cylinder (with a radius $a = w/2$) embedded in an infinite medium (solid line in Fig. 1d, with a slope of 0.582)[2, 5]. Since $p \propto R$, the linearity $N \propto p$ implies that the breakup wavelength $\lambda = 2\pi R/N \propto R/p$ was a constant for all the rings with sufficiently large p .

Besides λ , we were also interested in the phase correlation between the rupture of neighboring rings. To unambiguously identify the phase correlation, we statistical analyzed the coordinates of all the droplets formed. We define the phase shift (ϕ) *locally* for every droplet, as shown in Fig. 2a. For an arbitrary droplet X, we find its closest pair of droplets on the

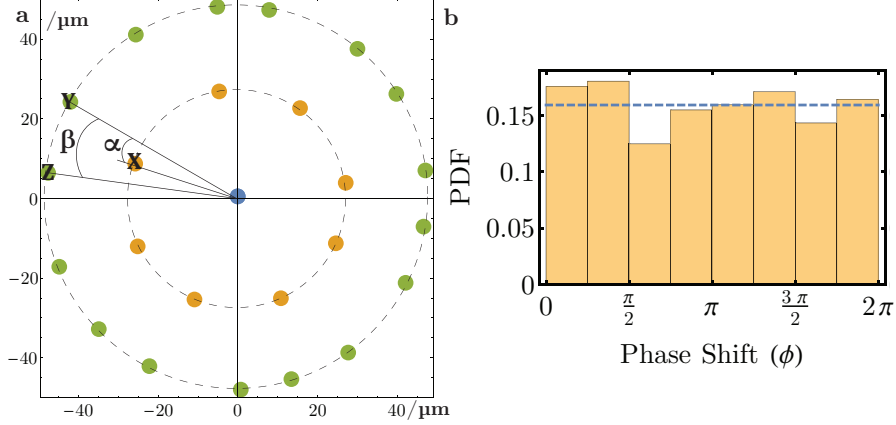


Figure 2. (a) Schematic for defining phase shift (ϕ); (b) Distribution of ϕ . The dashed line is the mean average of the bar heights.

outer ring, Y and Z, and calculate central angles α and β . We define ϕ with an angular relationship: $\phi = 2\pi\alpha/\beta$.

For in-phase correlation, X aligns with either Y or Z along the radius (in-phase), so ϕ becomes 0 or 2π , respectively. For out-of-phase, $\alpha = \beta/2$ and, therefore, $\phi = \pi$. Fig. 2f is the distribution across the entire sample, suggesting a uniform distribution: the rings ruptured independently. This is not surprising, given that neighboring rings are sparsely distanced ($2l/w \approx 13$). Knops et al. showed that for a viscosity ratio of 0.04, the flow induced by capillary rupture of a cylinder extended up to ~ 10 times its radius [4].

In order to enhance the hydrodynamic interference between neighboring rings, we fabricated Sample B with reduced l , via the same procedure but with a different mold (12 μm periodicity, and a line-and-space ratio of 1). Upon annealing at 170 $^\circ\text{C}$ for 5 min, the surface leveling process was completed, resulting in a set of denser packed rings (Fig. 3a) than Sample A (Fig. 1b). For Sample B: $w \approx 4.6 \mu\text{m}$, $h \approx 1.4 \mu\text{m}$, $h_r \approx 1.7 \mu\text{m}$ and $l \approx 12.1 \mu\text{m}$. The cross-section $w/h \approx 2.7$, again, reflected the balance between the γ_{PS} and $\gamma_{\text{PS/PMMA}}$. Most critically, the $2l/w$ ratio for Sample B was ~ 5.3 . Upon further annealing, the rings started to undulate and rupture (Fig. 3b). After 60 min, all rings had ruptured into discrete droplets (Fig. 3c), whose sizes and positions remained unchanged even after 540 min. (Fig. S3)

Similar as Sample A, the $N \sim p$ relationship (empty triangles in Fig. 1d) matched Tomotika's theory [2, 5]. The only exceptions are the two innermost rings, where in-plane relaxation dominated and reduced the number of droplets (arrows in Fig. 3b and Fig. 3c.)

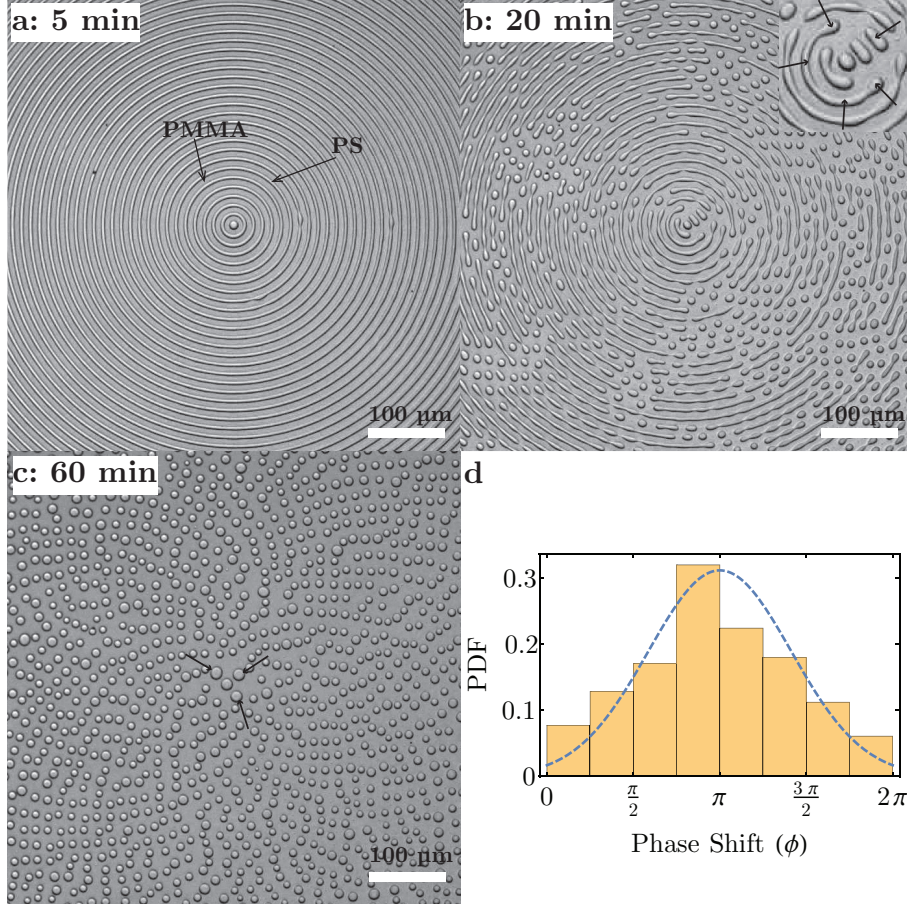


Figure 3. Optical images of Sample B annealed at 170 °C: (a) after leveling ($w = 4.6 \mu\text{m}$, $l = 12.1 \mu\text{m}$) and (b, c) rupture. (d) Distribution of ϕ . The dotted line is a fit to a truncated normal distribution within domain $[0, 2\pi)$.

In stark contrast, Fig. 3d suggested a unimodal distribution, peaked near π . This unambiguously shows that the most probable phase correlation is out-of-phase. For this sample, the neighboring rings were sufficiently near ($2l/w \approx 5.3$) to interfere with each other. Based on recent numerical work, for a cylinder/medium viscosity ratio of ~ 1 , out-of-phase correlation is expected for a $2l/w$ ratio of 3 – 10 [21]. Sample A and B had a $2l/w$ ratio of 12 and 5.3, consistent with their non-correlated or out-of-phase mode, respectively.

From the previous studies on *straight filaments* [3, 4, 15, 19], the out-of-phase mode is the result of synchronized flow amongst neighbors: An alternation of necking and expanding occurred along the orthogonal direction. Therefore, N is constrained to be identical between neighbors. If this is also true for *concentric rings*, it would contradict the observed $N \propto p$ (Fig. 1d). We owe the observed linearity to the locality of the out-of-phase breakup, since

there was no indication of long-range correlation/influence across Sample B surface (Fig. 3b and c). The correlation became more evident starting from the 6th ring (Fig. S4). This also resulted in a broadened distribution of ϕ .

Further decreasing the spacing between neighbors could transition the correlation into “in-phase”, when the axial flow started to couple amongst neighbors [4, 21]. This was also observed in sheared polymer blends [22]. From the recent numerical work [21], we expect the threshold of $2l/w$ for out-of-phase to in-phase transition to be ~ 3 , for our system (viscosity ratio of ~ 0.55). However, fabricating so densely-packed rings turned out rather challenging: Simply increasing the cast volume of PS (higher concentration or low spin speed) would only result in a thick top layer, which levels into a planar bilayer during annealing, as opposed to forming concentric rings [15].

We recently discovered that strongly confined straight filaments (e.g. small h_r) always break up in-phase, regardless of the viscosity ratio or the substrate wettability [23]. Herein, we fabricated substrate confined rings (Sample C). The degree of confinement can be defined as H/h , where H is the overall film thickness (Fig. 1a2). The smaller H/h is, the stronger substrate confinement is. The H/h for Sample A (Fig. 1) and B (Fig. 3) were 2.1 and 2.2, respectively; both were larger than the bulk-to-confinement threshold of 2.0 [24]. Therefore, both cases can be considered as weakly confined.

Fig. 4 shows Sample C (see Fig. S5 for more snapshots). After the initial surface leveling within 5 min (and stable up to 180 min), $w \approx 8.5 \mu\text{m}$, $h \approx 1.6 \mu\text{m}$, $h_r \approx 0.5 \mu\text{m}$, $l \approx 25.0 \mu\text{m}$. For Sample C, $H/h = 1.2$, meaning substrate exerted strong confinement on the rings. Its $w/h \approx 5.3$, indicating a flattened ribbon shape, that deviated significantly from the equilibrium shape ($w/h \approx 3$) of a weakly confined thread.

These confined rings were much more kinetically stable: they started to rupture between 400–600 min, which was more than one order of magnitude slower than Sample A and B (Fig. 4). The difference cannot be adequately explained by their difference in w . This is consistent with literature showing suppressed capillary instability under confinement [22, 25, 26]. Recent work by Alvine et al. also showed that the capillary fluctuations of polymer melt were dramatically hindered atop a topographic Si grating [27].

Despite the slow kinetics, the rings eventually ruptured (Fig. 4b). However, different from straight filament arrays [15, 23], these droplets radially lined up. We plot the $N \sim p$ scaling (diamond symbols) in Fig. 1d. The linearity again indicates constant λ for all rings.

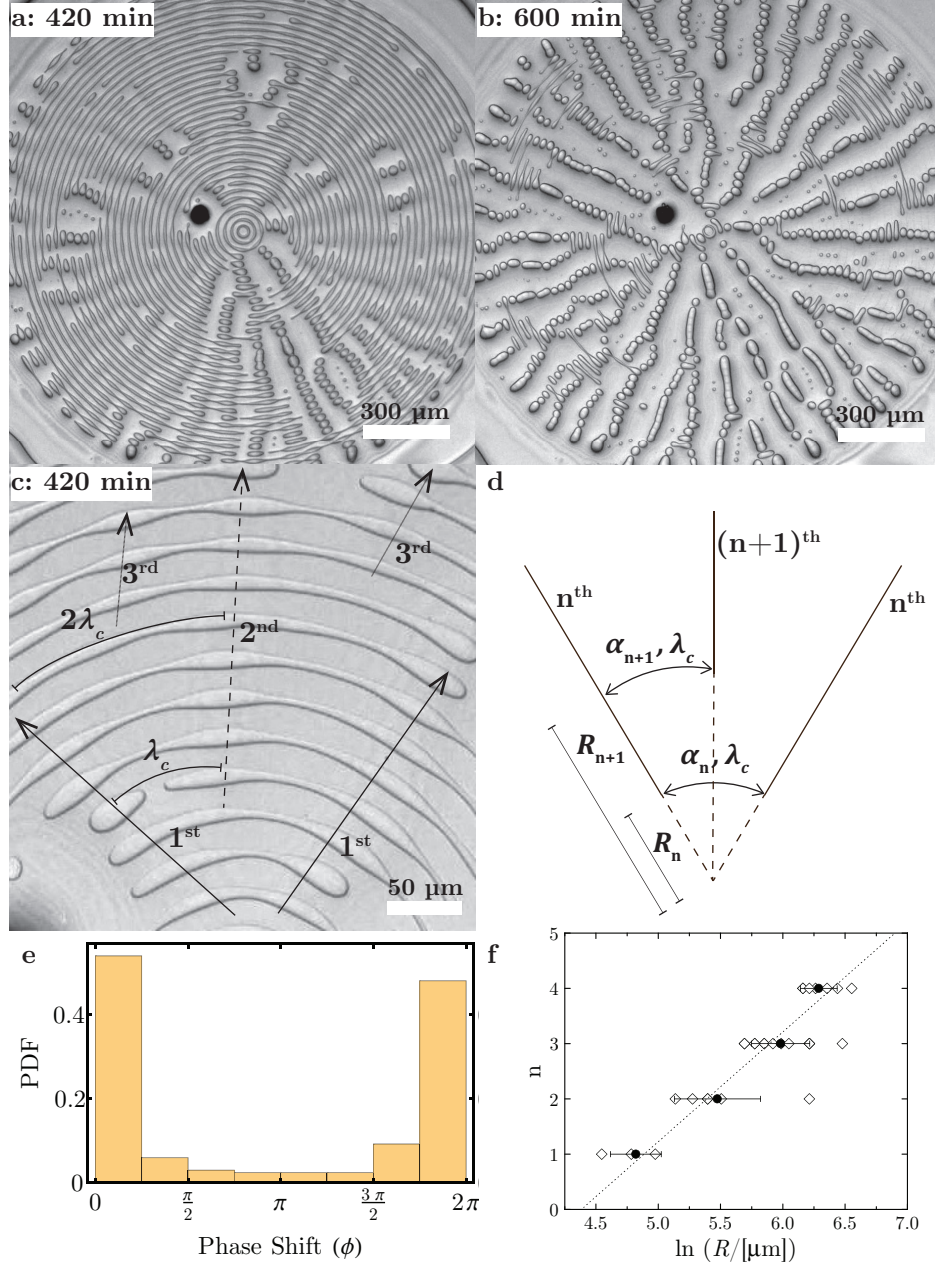


Figure 4. (a, b) Optical images of Sample C annealed at 170 °C for the labeled durations. Before undulation, $w = 8.5 \mu\text{m}$, $l = 25.0 \mu\text{m}$. (c) Close-up view of the undulation. (d) Schematic for the recursively “inserted” waves. (e) Distribution of ϕ . (f) Scaling between the order of generation n and R . Empty diamonds represent each new wave. The dotted line is a linear fit.

A linear fit (dotted line) shows that the slope (0.25) is less than half of Tomotika’s theory. This directly translates to larger wavelength and droplet size by volume conservation.

As previously discussed, for concentric rings, $N \propto p$ (also observed in two other strongly

confined patterns, Fig. S6). Apparently, more waves had been “inserted” into the outer rings. Here we attempt to shed light upon this process. Fig. 4(c) shows the undulation. The primary correlated directions are marked “1st(generation)”, extending radially from the center and perpendicular to the tangential of the rings. Moving away from the center, more waves were “inserted” in between the primary directions. Although the PS segments enveloped between “1st” directions all had the same central angle, their arc length (also λ) increased with R . The increased λ required a gradually less favorable undulation mode and built up the level of frustration. When this frustration grew sufficiently large, it could be released by inserting an additional wave in between (marked “2nd” in Fig. 4c). Similarly, the 3rd generation can be found at an even larger R .

Therefore, the most energetically favorable (least amount of frustration) mode should correspond to the smallest λ . We denote this characteristic wavelength with λ_c . The upper bound of λ should be the most frustrated wavelength $2\lambda_c$ (on the verge of splitting up into two waves). Thus we have $\lambda_c < \lambda < 2\lambda_c$. λ_c can be directly measured by identifying the smallest wavelength, as labeled in Fig. 4(c). We obtained that $\lambda_c = 77.8 \pm 11.0 \mu\text{m}$ and the average $\lambda = 108.9 \pm 7.0 \mu\text{m}$, which was consistent with the lower and upper bound limit. Tomotika’s theory provides a wavelength estimate of $45.9 \mu\text{m}$. However, the lower bound λ_c was larger than the prediction, due to confinement-induced wavelength increase [24, 26].

We develop a scaling relationship to capture the recursive nature of the “insertion” behavior. As shown in Fig. 4d, in between the n^{th} generation envelope (radius R_n , central angle α_n , wavelength λ_c), a new wave is inserted in the middle but at a larger radius R_{n+1} . Therefore, $\forall n \in \mathbb{N}$:

$$\alpha_n = \frac{\alpha_1}{2^{n-1}}, R_n \alpha_n = \lambda_c \implies R_n = \frac{\lambda_c}{2\alpha_1} \cdot 2^n \propto 2^n,$$

or equivalently $\ln R_n \propto n$. We statistically verify the scaling against the experimentally observed order of generation n and $\ln R_n$ (Fig. 4f and Supplementary Fig. S7). The dotted line is a fit to the mean value of $\ln R_n$ for each generation (n). The excellent linearity proves that, despite the randomness of surface capillary instability, our simple scaling analysis was capable of capturing the essential “recursive” behavior of the concentric rings.

In summary, we developed a novel procedure that allowed us to examine capillary breakup of concentrically arranged PS rings, suspended atop a layer of PMMA. When the substrate confinement was weak, the rings broke up independently if they were far apart, but via an

out-of-phase mode if they were sufficiently close. For both cases, the breakup wavelength agreed well with the prediction by Tomotika’s linear stability theory for a fully embedded cylinder (approximating the ring half-width as the cylinder radius). Under significant confinement of the substrate, the rings tended to breakup via an “in-phase” mode along the radial direction. The unique concentric ring geometry induced strong geometric frustration, which yielded a self-similar morphology that could be accounted for by our scaling analysis. Geometric frustration associated with curvature is a fundamentally important topic. Our experiments can serve as a basis for correlated capillary instability among curved objects, which can be a powerful tool for creating unique surface patterns.

This work was supported by the National Science Foundation under Grant CMMI-1031785 and CMMI-1233626. ZZ acknowledges support from the Beverly Sears Graduate Student Grant at CU-Boulder.

* Correspondence: yifu.ding@colorado.edu

- [1] J. Eggers and E. Villermaux, *Rep. Prog. Phys.* **71**, 036601 (2008).
- [2] S. Tomotika, *Proc. R. Soc. Lond. Ser. - Math. Phys. Sci.* **150**, 322 (1935).
- [3] P. H. M. Elemans, J. M. van Wunnik, and R. A. van Dam, *AIChE J.* **43**, 1649 (1997).
- [4] Y. M. M. Knops, J. J. M. Slot, P. H. M. Elemans, and M. J. H. Bulters, *AIChE J.* **47**, 1740 (2001).
- [5] E. Pairam and A. Fernández-Nieves, *Phys. Rev. Lett.* **102**, 234501 (2009).
- [6] Z. Yao and M. J. Bowick, *Eur. Phys. J. E* **34**, 1 (2011).
- [7] H. Mehrabian and J. J. Feng, *J. Fluid Mech.* **717**, 281 (2013).
- [8] E. Pairam, H. Le, and A. Fernández-Nieves, *Phys. Rev. E* **90**, 021002 (2014).
- [9] A. G. González, J. A. Diez, and L. Kondic, *J. Fluid Mech.* **718**, 246 (2013).
- [10] J. D. McGraw, J. Li, D. L. Tran, A.-C. Shi, and K. Dalnoki-Veress, *Soft Matter* **6**, 1258 (2010).
- [11] M. Byun, S. W. Hong, F. Qiu, Q. Zou, and Z. Lin, *Macromolecules* **41**, 9312 (2008).
- [12] Y. Wu, J. D. Fowlkes, P. D. Rack, J. A. Diez, and L. Kondic, *Langmuir* **26**, 11972 (2010).
- [13] T. D. Nguyen, M. Fuentes-Cabrera, J. D. Fowlkes, J. A. Diez, A. G. González, L. Kondic, and P. D. Rack, *Langmuir* **28**, 13960 (2012).

- [14] J. Lian, L. Wang, X. Sun, Q. Yu, and R. C. Ewing, *Nano Lett.* **6**, 1047 (2006).
- [15] Z. Zhang, D. U. Ahn, and Y. Ding, *Macromolecules* **45**, 1972 (2012).
- [16] Y. Ding, H. W. Ro, K. J. Alvine, B. C. Okerberg, J. Zhou, J. F. Douglas, A. Karim, and C. L. Soles, *Adv. Funct. Mater.* **18**, 1854 (2008).
- [17] Y. Ding, H. J. Qi, K. J. Alvine, H. W. Ro, D. U. Ahn, S. Lin-Gibson, J. F. Douglas, and C. L. Soles, *Macromolecules* **43**, 8191 (2010).
- [18] J. E. Mark, *Physical Properties of Polymers Handbook*, 2nd ed. (Springer, New York, 2007).
- [19] D. U. Ahn, Z. Wang, R. Yang, and Y. Ding, *Soft Matter* **6**, 4900 (2010).
- [20] D. U. Ahn and Y. Ding, *Soft Matter* **7**, 3794 (2011).
- [21] P. J. A. Janssen, H. E. H. Meijer, and P. D. Anderson, *Phys. Fluids* **24**, 012102 (2012).
- [22] N. S. Martys and J. F. Douglas, *Phys. Rev. E* **63**, 031205 (2001).
- [23] Z. Zhang, L. Wang, and Y. Ding, *Langmuir* **29**, 3073 (2013).
- [24] J. G. Hagedorn, N. S. Martys, and J. F. Douglas, *Phys. Rev. E* **69**, 056312 (2004).
- [25] K. B. Migler, *Physical Review Letters* **86**, 1023 (2001).
- [26] Y. Son, N. S. Martys, J. G. Hagedorn, and K. B. Migler, *Macromolecules* **36**, 5825 (2003).
- [27] K. J. Alvine, Y. Dai, H. W. Ro, S. Narayanan, A. R. Sandy, C. L. Soles, and O. G. Shpyrko, *Phys. Rev. Lett.* **109**, 207801 (2012).